45th AIAA/ASME/SAE/ASEE Joint Propulsion Conference & Exhibit
2 - 5 August 2009, Denver, Colorado

AIAA 2009-5306

Exact Eulerian Solution of the Conical Bidirectional Vortex

Timothy A. Barber* and Joseph Majdalani†
University of Tennessee Space Institute, Tullahoma, TN 37388

In this study, an exact Eulerian solution is derived for the bidirectional vortex in a conical chamber. Our model is applicable to idealized representations of cyclone separators and liquid rocket engines with slowly expanding chamber cross-sections. The bulk fluid motion is assumed to be nonreactive, steady, rotational, inviscid, and incompressible. Our approach is founded on the Bragg-Hawthorne equation and seeks to overcome some of the deficiencies encountered by Bloor and Ingham (Bloor, M. I. G., and Ingham, D. B., "The Flow in Industrial Cyclones," *Journal of Fluid Mechanics*, Vol. 178, 1987, pp. 507-519). Despite inevitable similarities with Bloor and Ingham's model, ours is constructed using a judicious framework that connects the solution to the swirl number and the cone divergence angle. In consequence, a self-similar formulation is produced that is independent of the cone's finite body length. This enables us able to characterize the problem by providing closed-form representations for the principal variables of flow motion. Among the parameters of interest, the mantle divergence angle and the maximum latitudinal velocity are obtained explicitly. The mantle consists of a spinning cone that separates the circumferential inflow region (outer vortex) from the central outflow (inner vortex). This interface bisects the fluid domain at 60% of the cone's divergence half-angle. Its precise determination helps to estimate the crossflow velocity responsible for mass transfer, or spillage as it were, from the outer vortex into the inner region. Finally, results are illustrated while varying the cone divergence angle and spatial location in both spherical and polar cylindrical coordinates.

Nomenclature

A_i	=	inlet area
a	=	outer injection radius, $L\tan\alpha$
b	=	inner injection radius, $L\tan\beta$
B	=	angular momentum as function of ψ, $R\sin\phi u_\theta$
H	=	stagnation pressure head
L	=	cone's vertical length
p	=	pressure
Q_i	=	inlet volumetric flow rate
R	=	radial spherical coordinate
r	=	radial (polar) cylindrical coordinate, $R\sin\phi$
$\boldsymbol{u}$	=	velocity, $\left(u_R, u_\phi, u_\theta\right)$
U	=	mean tangential (inflow) velocity
W	=	mean axial velocity
z	=	axial cylindrical coordinate

Greek

α	=	cone half-angle
β	=	mantle angle of inclination
Φ	=	tangent of half-angle, $\tan(\frac{1}{2}\phi)$
λ	=	constant, $\csc\alpha\tan(\frac{1}{2}\alpha)+\ln[\tan(\frac{1}{2}\alpha)]$

*Graduate Research Assistant, Mechanical, Aerospace and Biomedical Engineering Department. Member AIAA.
†H. H. Arnold Chair of Excellence in Advanced Propulsion, Mechanical, Aerospace and Biomedical Engineering Department. Senior Member AIAA. Fellow ASME.

ρ = density
σ_o = open area swirl number, $\left(a^2 - b^2\right)\big/A_i = U/(\pi W)$
ψ = stream function
ζ = ratio of axial to radial coordinates, z/r

Subscripts and Symbols
i = inlet property
o = outlet or open
R, ϕ, θ = radial, colatitude, or azimuthal component
r, z, θ = radial, axial, or azimuthal component

I. Introduction

INTEREST in modeling cyclonic motions has been recently revived, especially in propulsive applications where swirl-driven cyclones have become known for their elevated efficiencies and self-cooling properties. In fact, several types of liquid[1-11] and hybrid[1-9] rocket engines under development today are based on the so-called bidirectional vortex. This bipolar vortex denotes a cyclone comprising a pair of (outer and inner) coaxial, co-rotating swirling streams that are separated by a spinning wheel known as the mantle. The latter constitutes a rotating, non-translating shear layer along which mass can cross inwardly from the outer, annular vortex to the inner, central core where combustion and/or mixing can be vigorously promoted.

Using cylindrical combustion chambers, analytical models have been advanced by Vyas and Majdalani,[10] Majdalani and Rienstra,[11] and Vyas, Majdalani and Chiaverini[12-14] for the liquid engine application, and by Majdalani[15] for the hybrid engine case. Cold flow experimentation using PIV[16-17] and numerical models have also been implemented under both cold[18] and reactive flow conditions.[19]

From a historical perspective, the bidirectional vortex concept that is now applied to liquid and hybrid thrust engines was first implemented in industrial cyclones. In fact, one of the earliest analyses may be traced back to ter Linden's experimental work on dust separators in the late 1940s.[20] Both hydraulic and gaseous cyclones were also investigated by Kelsall[21] and Smith,[22-23] respectively. Work on conical dust separators continues today as documented in the comprehensive studies by Peng, Hoffmann and Dries,[24] Hu *et al.*,[25] Cortes and Gil,[26] and others.

For the conical cyclone, the earliest theoretical analysis may be attributed to Fontein and Dijksman[27] who once evoked semi-empirical approaches and curve fitting to obtain physically viable approximations.[27] A more refined model based on the Polhausen method was later suggested by Bloor and Ingham[28] and shown to be in fair agreement with Kelsall's measurements.[21] A more useful approximation for the conical cyclone would later emerge from the work of Bloor and Ingham;[29] this time, they were able to incorporate realistic boundary conditions into their inviscid model. At the outset, their solution was useful in reproducing the overall features of the flow simulated numerically by Hsieh and Rajamani,[30] Hoekstra, Derksen and Van den Akker,[31] and Derksen and Van den Akker.[32] Bloor and Ingham's approach was based on the Bragg-Hawthorne equation and appropriate assumptions concerning the conservation of enthalpy and angular momentum along inlet flow streamlines.[29]

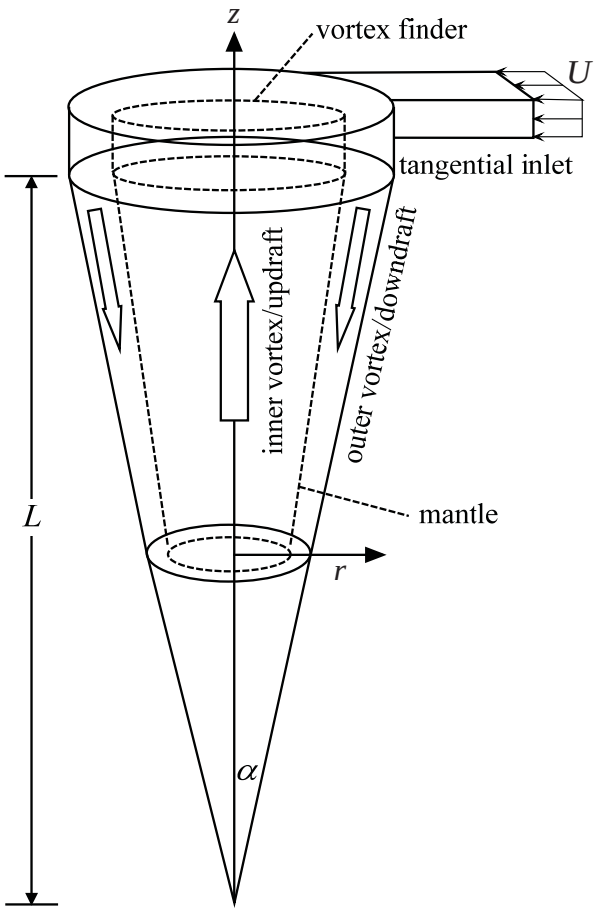

Figure 1. Schematic of a conical cyclone separator.

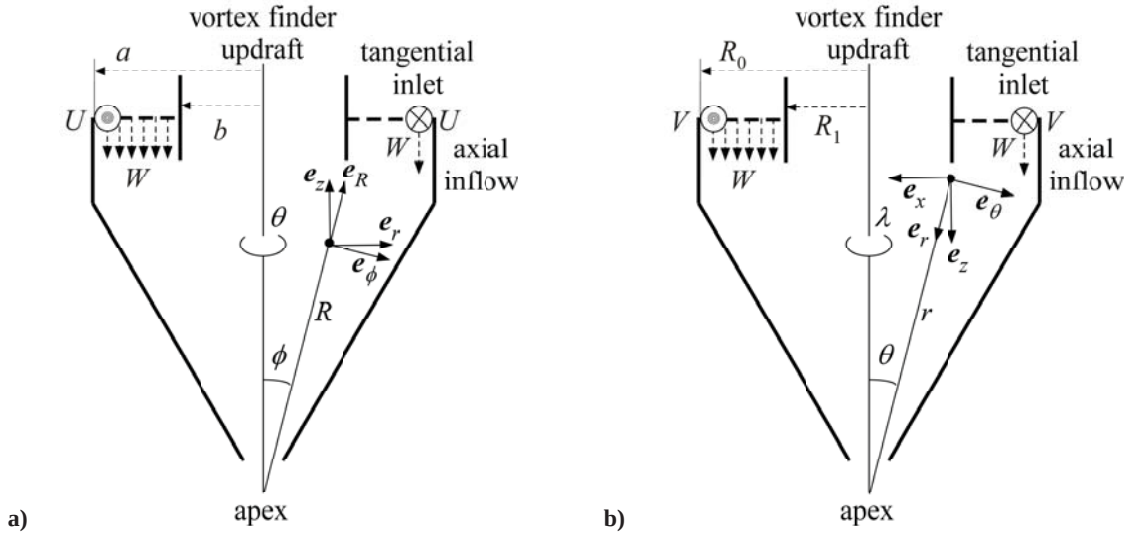

Figure 2. Geometric model and coordinate systems used in a) the present analysis and b) Bloor and Ingham's.[29]

Other studies, such as those by Zhao and Abrahamson,[33] sought to demonstrate the effect of the upstream boundary conditions in the presence of a vortex finder. Consideration was also given to the differences between axial and slotted injection. While some numerical studies explored the effect of geometry on the separation efficiency[20] and/or the performance of cyclone separators,[24-26] others sought to analyze their instability.[22-23]

Considering that the conical chamber is of key relevance to both industrial cyclones and modern concepts of liquid and hybrid engines, it is the purpose of this paper to derive an exact solution for the bidirectional vortex in a conical setting. Using a judicious choice of spherical coordinates, our approach will extend and complement the work of Bloor and Ingham[29] by revisiting the Bragg-Hawthorne equation from which a verifiable inviscid solution may be obtained. In a companion paper,[34] the same approach will be applied to the cylindrical chamber for which new exact solutions will be derived under isentropic conditions. Not only will our solutions be shown to satisfy Euler's equation identically, but they will also exhibit the key characteristic parameters, such as the swirl number, that will permit reconciliation with other exact solutions in the literature.[11]

II. Problem Formulation

A. Geometry

Our cyclonic separator is presented as an idealized cone with a divergence half-angle α and length L. The schematic shown in Fig. 1 incorporates both the divergent body and the non-divergent cylindrical segment termed *vortex finder*. Our analysis is limited to the divergent segment of this device as the vortex finder plays the role of an outlet nozzle in a conical thrust chamber. Whether using cylindrical or spherical coordinates, the origin of the reference frame is anchored at the apex of the cone (or the bottom-center of the chamber, in the case of a cylinder). Mass addition takes place tangentially at an average injection speed of U and volumetric flowrate Q_i. The injected stream then turns axially, thus forming a downdraft at an average axial velocity of W. This inwardly directed stream generates the outer vortex by filling the annular region extending from the mantle to the wall. Inside the mantle, an inner vortex is formed through which fluid is carried upwardly and out of the chamber. In this study, we are not concerned with the three-dimensional development of the tangential source into an axial stream. We assume that the flow turning process is immediate. As for the outer vortex in the exit plane, it is bounded by the inner and outer radii, b and a. As shown in Fig. 2a, we use a right-handed coordinate system consisting of a spherical radius R, a colatitude angle ϕ, and an azimuthal angle θ defined positive in the direction of swirl.

B. Spherical Equations and Assumptions

For the present model, the flow can be characterized as (i) steady, (ii) inviscid, (iii) incompressible, (iv) rotational, and (v) non-reactive. When these assumptions enforced, the conservation of mass and momentum equations become

$$\frac{1}{R^2}\ \frac{\partial}{\partial R}\left(u_R R^2\right)+\frac{1}{R\sin\phi}\frac{\partial}{\partial\phi}\left(u_\phi\sin\phi\right)+\frac{1}{R\sin\phi}\frac{\partial}{\partial\theta}\left(u_\theta\right)=0 \tag{1}$$

for continuity, and for Euler's spherical equations,

$$\begin{cases} u_R\dfrac{\partial u_R}{\partial R}+\dfrac{u_\phi}{R}\dfrac{\partial u_R}{\partial\phi}+\dfrac{u_\theta}{R\sin\phi}\dfrac{\partial u_R}{\partial\theta}-\dfrac{u_\phi^2+u_\theta^2}{R}=-\dfrac{1}{\rho}\dfrac{\partial p}{\partial R} \\ u_R\dfrac{\partial u_\phi}{\partial R}+\dfrac{u_\phi}{R}\dfrac{\partial u_\phi}{\partial\phi}+\dfrac{u_\theta}{R\sin\phi}\dfrac{\partial u_\phi}{\partial\theta}+\dfrac{u_R u_\phi}{R}-\dfrac{u_\theta^2\cot\phi}{R}=-\dfrac{1}{\rho R}\dfrac{\partial p}{\partial\phi} \\ u_R\dfrac{\partial u_\theta}{\partial R}+\dfrac{u_\phi}{R}\dfrac{\partial u_\theta}{\partial\phi}+\dfrac{u_\theta}{R\sin\phi}\dfrac{\partial u_\theta}{\partial\theta}+\dfrac{u_R u_\theta}{R}+\dfrac{u_\phi u_\theta}{R}\cot\phi=-\dfrac{1}{\rho R\sin\phi}\dfrac{\partial p}{\partial\theta} \end{cases} \tag{2}$$

In conformance with the theory of laminar swirling flows, the absence of friction enables us to justify the use of axisymmetry about the vertical axis. This reduces Eqs. (1)-(2) into

$$\frac{\partial}{\partial R}\left(u_R R^2\sin\phi\right)+\frac{\partial}{\partial\phi}\left(u_\phi R\sin\phi\right)=0 \quad \text{(continuity)} \tag{3}$$

$$u_R\frac{\partial u_R}{\partial R}+\frac{u_\phi}{R}\frac{\partial u_R}{\partial\phi}-\frac{u_\phi^2+u_\theta^2}{R}=-\frac{1}{\rho}\frac{\partial p}{\partial R} \quad \text{(radial)} \tag{4}$$

$$u_R\frac{\partial u_\phi}{\partial R}+\frac{u_\phi}{R}\frac{\partial u_\phi}{\partial\phi}+\frac{u_R u_\phi}{R}-\frac{u_\theta^2\cot\phi}{R}=-\frac{1}{\rho R}\frac{\partial p}{\partial\phi} \quad \text{(latitudinal)} \tag{5}$$

$$u_R\frac{\partial u_\theta}{\partial R}+\frac{u_\phi}{R}\frac{\partial u_\theta}{\partial\phi}+\frac{u_R u_\theta}{R}+\frac{u_\phi u_\theta}{R}\cot\phi=0 \quad \text{(azimuthal)} \tag{6}$$

with vorticity being expressible by

$$\boldsymbol{\omega}=\frac{1}{R\sin\phi}\frac{\partial}{\partial\phi}\left(u_\theta\sin\phi\right)\boldsymbol{e}_R-\frac{1}{R}\frac{\partial}{\partial R}\left(Ru_\theta\right)\boldsymbol{e}_\phi+\frac{1}{R}\left[\frac{\partial}{\partial R}\left(Ru_\phi\right)-\frac{\partial u_R}{\partial\phi}\right]\boldsymbol{e}_\theta \tag{7}$$

The importance of this relationship will soon be established.

C. Boundary Conditions

Given axisymmetric condition with respect to the azimuth, our conical flow field can be made to satisfy two conditions on the stream function, $\psi\left(R,\phi\right)$. By insisting that the stream function vanishes at both the centerline and the conical wall (at $\phi=\alpha$), we set

$$\psi\left(R,0\right)=\psi\left(R,\alpha\right)=0 \tag{8}$$

Furthermore, we assume that the tangential inlet is responsible for mass added to the chamber. We thus let

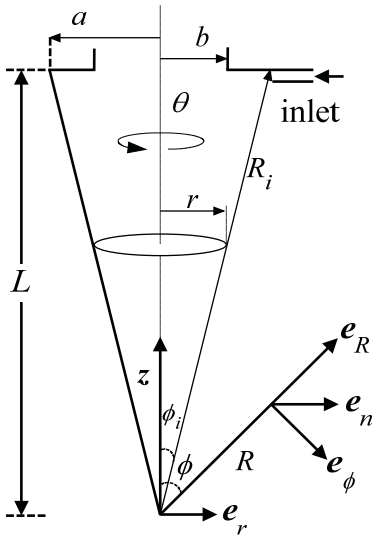

Figure 3. Spherical radius and colatitude angle corresponding to inlet conditions.

$$Q_i = u_\theta\left(R_i, \phi_i\right) = UA_i \tag{9}$$

where the spherical radius and colatitude angle corresponding to inlet conditions are given by (see Fig. 3)

$$\phi_i = \alpha = \tan^{-1}\left(a/L\right); \qquad R_i = \sqrt{L^2 + a^2} \tag{10}$$

We also assume that the tangential injected flow is responsible for producing the entire flow into the annular section of the outer vortex (downdraft shown in Fig. 1). Finally, we verify that mass balance between the outer, annular vortex and inner, core vortex is maintained. By integrating the solution over the inlet and outlet sections, we set to confirm that $Q_o = Q_i = UA_i$.

III. Procedure

A. Streamline Projection

We begin by using Lamb's vector identity $\left(\boldsymbol{u}\cdot\nabla\right)\boldsymbol{u} = \nabla\left(\frac{1}{2}\boldsymbol{u}\cdot\boldsymbol{u}\right) - \boldsymbol{u}\times\left(\nabla\times\boldsymbol{u}\right)$ to transform the convective term in the Euler's equation, specifically, in $\left(\boldsymbol{u}\cdot\nabla\right)\boldsymbol{u} = -\nabla p/\rho$. The momentum equations becomes

$$\nabla \mathrm{H} - \boldsymbol{u}\times\boldsymbol{\omega} = 0; \quad \mathrm{H} = \tfrac{1}{2}u^2 + p/\rho z \tag{11}$$

where H is the fluid head. Based on the stream function $\psi\left(R,\phi\right)$, the radial and colatitude velocities may be expressed as

$$u_R = \frac{1}{R^2\sin\phi}\frac{\partial\psi}{\partial\phi} \tag{12}$$

$$u_\phi = -\frac{1}{R\sin\phi}\frac{\partial\psi}{\partial R} \tag{13}$$

Considering a flow displacement $\mathrm{d}\boldsymbol{s}$ we then project the momentum equation along a streamline. This enables us to write

$$\nabla \mathrm{H}\cdot\mathrm{d}\boldsymbol{s} - \left(\boldsymbol{u}\times\boldsymbol{\omega}\right)\cdot\mathrm{d}\boldsymbol{s} = 0 \qquad \text{or} \qquad \nabla \mathrm{H}\cdot\mathrm{d}\boldsymbol{s} = 0 \tag{14}$$

The pressure head is then obtained by integrating Eq. (14) along a streamline. We recover Bernoulli's form

$$\mathrm{H}\left(\psi\right) = \tfrac{1}{2}u^2 + p/\rho \tag{15}$$

where $\mathrm{H}\left(\psi\right)$ is constant along each streamline. This basic derivation is intended to clarify the origin of $\mathrm{H}\left(\psi\right)$ which arises in the Bragg-Hawthorne equation.

B. Swirl Velocity

Based on the $\theta-$ momentum equation, we group $u_\theta R\sin\phi$ and reduce Eq. (6) into

$$\frac{u_\phi}{R}\frac{\partial}{\partial\phi}\left(u_\theta R\sin\phi\right) + u_R\frac{\partial}{\partial R}\left(u_\theta R\sin\phi\right) = 0 \qquad \text{or} \qquad \frac{\mathrm{d}}{\mathrm{d}t}\left(u_\theta R\sin\phi\right) = 0 \tag{16}$$

The material derivative directly leads to the tangential velocity,

$$u_\theta R\sin\phi = \mathrm{B}\left(\psi\right) \qquad \text{or} \qquad u_\theta = \frac{\mathrm{B}\left(\psi\right)}{R\sin\phi} \tag{17}$$

where $\mathrm{B}\left(\psi\right)$ is a form of tangential angular momentum that is to yet to be determined.

C. Radial and Tangential Vorticity Relations

Using the free vortex relation for the tangential velocity, $\mathrm{B}\left(\psi\right)$ may be connected to the radial vorticity, ω_R. By substituting u_θ into Eq. (7), we retrieve

$$\omega_R = \frac{1}{R^2\sin\phi}\frac{\partial \mathrm{B}}{\partial\phi} = \frac{1}{R^2\sin\phi}\frac{\mathrm{dB}}{\mathrm{d}\psi}\frac{\partial\psi}{\partial\phi} \tag{18}$$

where the derivative with respect to the stream function is deliberately used in view of $\mathrm{B} = \mathrm{B}(\psi)$.

Next, the tangential vorticity may be extracted from the $\phi-$momentum equation. Transforming Eq. (11) into scalar form, we segregate the ϕ component and rewrite it as

$$\frac{1}{R}\frac{\mathrm{dH}}{\mathrm{d}\psi}\frac{\partial\psi}{\partial\phi} + u_R\omega_\theta - u_\theta\omega_R = 0 \tag{19}$$

Making the necessary substitutions for the radial and tangential velocities as well as the radial vorticity, we are left with

$$\frac{1}{R}\frac{\partial \mathrm{H}}{\partial \psi}\frac{\partial \psi}{\partial \phi}+\frac{1}{R^2\sin\phi}\frac{\partial \psi}{\partial \phi}\omega_\theta-\frac{\mathrm{B}(\psi)}{R\sin\phi}\left(\frac{1}{R^2\sin\theta}\frac{\mathrm{dB}}{\mathrm{d}\psi}\frac{\partial \psi}{\partial \phi}\right)=0 \tag{20}$$

This expression may be considerably simplified and rearranged into

$$\frac{\omega_\theta}{R\sin\phi}=\frac{1}{R^2\sin^2\phi}\mathrm{B}\frac{\mathrm{dB}}{\mathrm{d}\psi}-\frac{\mathrm{dH}}{\mathrm{d}\psi} \tag{21}$$

D. Bragg-Hawthorne Equation

After inserting the tangential vorticity of Eq. (7) into Eq. (21), the velocities may be eliminated through Eqs. (12) -(13). The outcome is a form of the Bragg-Hawthorne equation (BHE) in spherical coordinates. We obtain

$$\frac{1}{R}\left[\frac{\partial}{\partial R}\left(-\frac{1}{\sin\phi}\frac{\partial \psi}{\partial R}\right)-\frac{\partial}{\partial \phi}\left(\frac{1}{R^2\sin\phi}\frac{\partial \psi}{\partial \phi}\right)\right]=\frac{1}{R\sin\phi}\mathrm{B}\frac{\mathrm{dB}}{\mathrm{d}\psi}-R\sin\phi\frac{\mathrm{dH}}{\mathrm{d}\psi} \tag{22}$$

and so

$$\frac{\partial^2\psi}{\partial R^2}+\frac{\sin\phi}{R^2}\frac{\partial}{\partial \phi}\left(\frac{1}{\sin\phi}\frac{\partial \psi}{\partial \phi}\right)=R^2\sin^2\phi\frac{\mathrm{dH}}{\mathrm{d}\psi}-\mathrm{B}\frac{\mathrm{dB}}{\mathrm{d}\psi}\quad\text{(Bragg-Hawthorne)} \tag{23}$$

Clearly, the proper choice of $\mathrm{B}(\psi)$ and $\mathrm{H}(\psi)$ will be instrumental to the solution of Eq. (23).

IV. Solution

A. Axial Inlet Conditions

The flow injected tangentially along the periphery must turn inwardly. We therefore take W as the average axial velocity at entry, where $b\le r\le a$, b being the inner radius of the open gap shown in Fig. 3. The stream function corresponding to a top hat profile is well known to be $\mathrm{d}\psi/\mathrm{d}(R\sin\phi)=WR\sin\phi$. Hence,

$$\psi=\tfrac{1}{2}W\left(R^2\sin^2\phi-a^2\right) \tag{24}$$

where through our choice the integrating constant makes the stream function equal to zero at the wall. The volumetric flow rate at the inlet then equals

$$Q_i=\pi\left(a^2-b^2\right)W \tag{25}$$

Note that the inlet stream function is simply a uniform velocity profile in spherical coordinates. This approach enables us to introduce an inlet boundary condition that will disseminate throughout the chamber.

B. Relations for B and H

In order to link $\mathrm{B}(\psi)$ and $\mathrm{H}(\psi)$, we consider the inlet condition where the tangential velocity enters at an average velocity of U. Equation (17) becomes, along the inlet section,

$$UR\sin\phi=\mathrm{B}(\psi) \tag{26}$$

where B remains constant along a streamline. Next we differentiate Eqs. (24) and (26) with respect to $R\sin\phi$ to obtain, at the top of the cone,

$$\frac{\mathrm{dB}}{\mathrm{d}(R\sin\phi)}=U \tag{27}$$

A combination of these two expressions leads to

$$\mathrm{B}\frac{\mathrm{dB}}{\mathrm{d}\psi}=\frac{UR\sin\phi}{WR\sin\phi}U=\frac{U^2}{W}=\text{const.} \tag{28}$$

This relation grants the tangential velocity the freedom to vary with the stream function. The total velocity at entry is hence $\sqrt{u_r^2(R_i,\phi_i)+U^2+W^2}$ (see Fig. 3). Assuming a constant inlet velocity, we may revisit Eq. (15) and write

$$\mathrm{H}=\tfrac{1}{2}\left[u_r^2(R_i,\phi_i)+U^2+W^2\right]+p_0/\rho=\text{const}\quad\text{or}\quad\frac{\mathrm{dH}}{\mathrm{d}\psi}=0 \tag{29}$$

Note that the flow in question is isentropic to the extent that the total enthalpy variation reduces to that of the stagnation pressure head (Bragg and Hawthorne[35]). The substitution of Eqs. (28) and (29) into BHE reduce it into

$$\frac{\partial^2\psi}{\partial R^2}+\frac{\sin\phi}{R^2}\frac{\partial}{\partial\phi}\left(\frac{1}{\sin\phi}\frac{\partial\psi}{\partial\phi}\right)=-\frac{U^2}{W} \tag{30}$$

C. Stream Function Representation

In seeking an exact solution, we attempt separation of variables and posit the ansatz,[29]

$$\psi=R^2F(\phi) \tag{31}$$

Substituting this form into Eq. (30) gives rise to a second order ODE, specifically,

$$2F+\sin\phi\frac{\mathrm{d}}{\mathrm{d}\phi}\left(\frac{1}{\sin\phi}\frac{\mathrm{d}F}{\mathrm{d}\phi}\right)=-\frac{U^2}{W} \tag{32}$$

The solution to Eq. (32) may be obtained by setting

$$F=f(\phi)\sin^2\phi-\tfrac{1}{2}U^2W^{-1} \tag{33}$$

which readily produces

$$f(\phi)=-\frac{1}{2}\left[\csc\phi\cot\phi+\ln\left(\csc\phi+\cot\phi\right)\right] \tag{34}$$

and so

$$F=-\frac{U^2}{2W}+K_1\sin^2\phi+K_2\left[\cos\phi-\left(\sin^2\phi\right)\ln\Phi\right] \tag{35}$$

where $\Phi\equiv\tan\left(\tfrac{1}{2}\phi\right)$.

As usual, we fix the stream function at the axis of symmetry and the sidewall. Using $\psi(R,0)=\psi(R,\alpha)=0$, we deduce

$$F(0)=F(\alpha)=0 \tag{36}$$

Both K_1 and K_2 can be collected, namely,

$$\begin{cases}K_1=\dfrac{U^2}{2W}\left\{\csc^2\alpha+\ln\left[\tan\left(\tfrac{1}{2}\alpha\right)\right]-\csc\alpha\cot\alpha\right\}=\dfrac{U^2}{2W}\left\{\csc\alpha\tan\left(\tfrac{1}{2}\alpha\right)+\ln\left[\tan\left(\tfrac{1}{2}\alpha\right)\right]\right\}\\ K_2=\dfrac{U^2}{2W}\end{cases} \tag{37}$$

At this point, we define

$$\lambda\equiv K_1\frac{2W}{U^2}=\csc\alpha\left(\csc\alpha-\cot\alpha\right)+\ln\left[\tan\left(\tfrac{1}{2}\alpha\right)\right]=\csc\alpha\tan\left(\tfrac{1}{2}\alpha\right)+\ln\left[\tan\left(\tfrac{1}{2}\alpha\right)\right] \tag{38}$$

This enables us to collapse Eq. (35) into

$$F=\frac{U^2}{2W}\left[\left(\lambda-\ln\Phi\right)\sin^2\phi+\cos\phi-1\right]=\frac{U^2\sin^2\phi}{2W}\left(\lambda-\ln\Phi+\csc\phi\cot\phi-\csc^2\phi\right) \tag{39}$$

and

$$\psi=\frac{U^2R^2}{2W}\left[\left(\lambda-\ln\Phi\right)\sin^2\phi+\cos\phi-1\right]=\frac{U^2R^2\sin^2\phi}{2W}\left(\lambda-\ln\Phi-\Phi\csc\phi\right) \tag{40}$$

D. Velocities

With the stream function at hand, the radial and latitudinal velocities, u_R and u_ϕ, may be extracted. Through proper differentiation, we obtain

$$\begin{cases}u_R=\dfrac{U^2}{W}\left[\left(\lambda-\ln\Phi\right)\cos\phi-1\right]\\ u_\phi=-\dfrac{2\psi}{R^2\sin\phi}=\dfrac{U^2}{W}\left[\left(\ln\Phi-\lambda\right)\sin\phi+\Phi\right]\end{cases} \tag{41}$$

To produce the tangential velocity, we use Eq. (28) and solve for B. Integration renders

$$\int \mathrm{B}\,\mathrm{dB} = \int \frac{U^2}{W}\,\mathrm{d}\psi \qquad \text{or} \qquad \mathrm{B}(\psi) = \sqrt{2\frac{U^2}{W}\psi + \mathrm{B}_1} \tag{42}$$

At the inlet, $\psi = \frac{1}{2}W\left(R^2\sin^2\phi - a^2\right)$, which, when substituted into Eq. (42), yields

$$UR\sin\phi = \sqrt{2\frac{U^2}{W}\left[\tfrac{1}{2}W\left(R^2\sin^2\phi - a^2\right)\right] + \mathrm{B}_1} \qquad \text{or} \qquad \mathrm{B}_1 = a^2U^2 \tag{43}$$

Hence we have

$$\frac{\mathrm{B}(\psi)}{Ua} = \sqrt{1 + 2\frac{\psi}{Wa^2}} \tag{44}$$

Next, we may substitute into Eq. (17) to obtain

$$\frac{u_\theta}{U} = \frac{a}{R\sin\phi}\sqrt{1 + \frac{2\psi}{Wa^2}} \tag{45}$$

Note that one recovers $u_\theta = U$ along the inlet section where a uniform flow prevails. Finally, using the actual stream function inside the cone, we retrieve,

$$\frac{u_\theta}{U} = \frac{a}{R\sin\phi}\sqrt{1 + \left(\frac{UR\sin\phi}{Wa}\right)^2\left(\lambda - \ln\Phi - \Phi\csc\phi\right)} \tag{46}$$

Compared to the free vortex solution of Vyas and Majdalani[10] the tangential velocity obtained using this approach continues to retain the general free vortex form requiring inverse variation with the distance from the axis of rotation $\sim (R\sin\phi)^{-1}$. In addition, however, it exhibits a crucial dependence on the inlet velocity profile and the spatially varying stream function. It can therefore be seen that the characteristics features of this procedure consist of (i) retaining the spatial dependence through the stream function and (ii) accounting for a specific axial injection profile at entry. These important steps can be systematically applied to other geometric settings as it will be shown in the companion paper by Majdalani.[34]

V. Results and Discussion

A. Conical Swirl Number

Through the use of Eq. (25), the inlet axial velocity W may be eliminated in favor of the actual tangential flow rate into the chamber,

$$W = \frac{Q_i}{\pi\left(a^2 - b^2\right)} = \frac{UA_i}{\pi\left(a^2 - b^2\right)} \tag{47}$$

This key substitution gives rise to a modified form of the swirl number that is applicable to our conical model.[31] We thus define,

$$\sigma_o \equiv \frac{a^2 - b^2}{A_i} = \frac{L^2}{A_i}\left(\tan^2\alpha - \tan^2\beta\right) = \frac{U}{\pi W} \tag{48}$$

where β denotes the divergence angle of the mantle, and $W = U\sigma_o/\pi$. Forthwith, the stream function becomes

$$\psi = \tfrac{1}{2}\pi\sigma_o UR^2\left[\sin^2\phi\left(\lambda - \ln\Phi\right) + \cos\phi - 1\right] = \tfrac{1}{2}\pi\sigma_o UR^2\sin^2\phi\left(\lambda - \ln\Phi - \Phi\csc\phi\right) \tag{49}$$

The companion velocities can be similarly expressed as

$$u_R = \pi\sigma_o U\left[\left(\lambda - \ln\Phi\right)\cos\phi - 1\right] \tag{50}$$

$$u_\phi = -\pi\sigma_o U\left[\left(\lambda - \ln\Phi\right)\sin\phi - \Phi\right] \tag{51}$$

$$u_\theta = \frac{Ua}{R\sin\phi}\sqrt{1 + \left(\frac{\sigma_o\pi R\sin\phi}{a}\right)^2\left(\lambda - \ln\Phi - \Phi\csc\phi\right)} \tag{52}$$

This completes our solution in spherical coordinates.

B. Normalization

With the focus being directed to a full cone, we can use the trigonometric replacement, $a_o = L\tan\alpha$. Inserting this expression into the tangential velocity equation yields

$$u_\theta = \frac{UL\tan\alpha}{R\sin\phi}\sqrt{1+\left(\frac{\sigma_o \pi R\sin\phi}{L\tan\alpha}\right)^2\left(\lambda - \ln\Phi - \Phi\csc\phi\right)} \tag{53}$$

Equation (53) can be used to guide our normalization. We do so while attempting to adhere with the nomenclature used in similar contexts, such as those by Majdalani and Rienstra.[11] We therefore take

$$\bar{R} = \frac{R}{a};\quad \bar{\psi} = \frac{\psi}{Ua^2};\quad \bar{\mathrm{B}}(\bar{\psi}) = \frac{\mathrm{B}(\psi)}{Ua};\quad \bar{\mathrm{H}}(\bar{\psi}) = \frac{\mathrm{H}(\psi)}{U^2} \tag{54}$$

$$\bar{u}_R = \frac{u_R}{U};\quad \bar{u}_\phi = \frac{u_\phi}{U};\quad \bar{u}_\theta = \frac{u_\theta}{U};\quad \bar{Q}_i = \frac{Q_i}{U\left(a^2-b^2\right)} = \frac{A_i}{a^2-b^2} = \frac{\pi W}{U} = \sigma_o^{-1} \tag{55}$$

where a is the maximum radius of the cone. Given geometric similarity at fixed divergence angle, L can be shown to disappear in a judiciously normalized system, although results can be presented for a unit chamber length

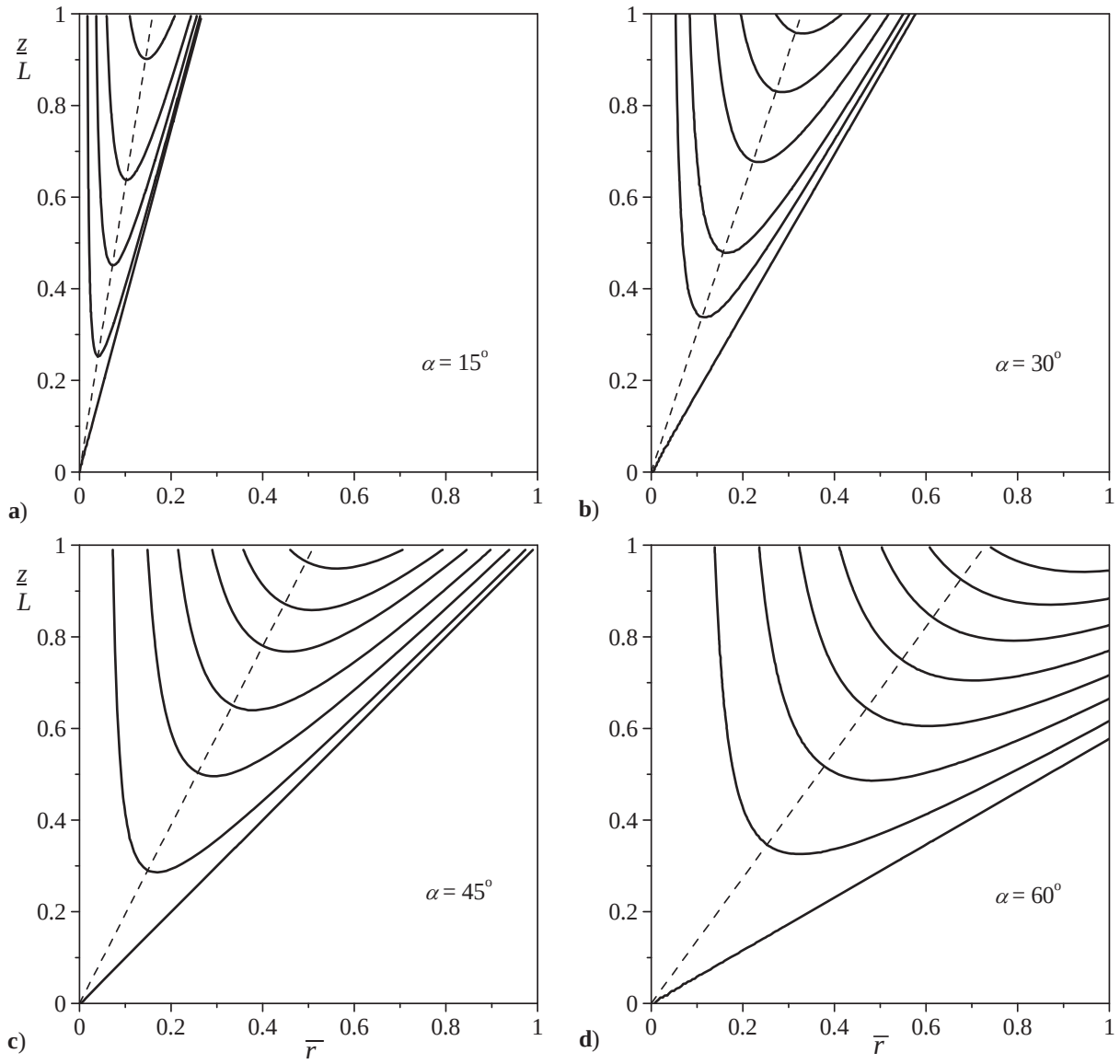

Figure 4. Cyclonic flow streamlines shown for σ_o = 1 and a) α = 15°, b) 30°, c) 45°, and d) 60°.

($L = 1$). Note that from this point forward, all of our dimensionless variables are tagged with overbars except for the angle variables. The dimensionless forms reduce to

$$\bar{\psi} = \tfrac{1}{2}\pi\sigma_o \bar{R}^2 \sin^2\phi\left(\lambda - \ln\Phi - \Phi\csc\phi\right); \quad \bar{\mathrm{B}}(\bar{\psi}) = \left(\bar{R}\sin\phi\,\bar{u}_\theta\right) = \sqrt{1 + 2\pi\sigma_o\bar{\psi}} \tag{56}$$

$$\bar{u}_R = \pi\sigma_o\left[\left(\lambda - \ln\Phi\right)\cos\phi - 1\right] \tag{57}$$

$$\bar{u}_\phi = -\pi\sigma_o\left[\left(\lambda - \ln\Phi\right)\sin\phi - \Phi\right] \tag{58}$$

$$\bar{u}_\theta = \frac{1}{\bar{R}\sin\phi}\sqrt{1 + {\sigma_o}^2\pi^2\bar{R}^2\sin^2\phi\left(\lambda - \ln\Phi - \Phi\csc\phi\right)} \tag{59}$$

The streamlines prescribed by Eq. (56) are shown in Fig. 4 at four different cone half-angles of 15, 30, 45, and 60 degrees. In these plots, the outer and inner vortex regions are separated by a broken line that corresponds to the mantle location. The contour curves represent lines of constant ψ, thus illustrating the downdraft, bending, and updraft regions.

C. Mantle Location

In order to determine the mantle location, we consider the behavior of the radial velocity $\bar{u}_R$ in and out of the cyclone. Theoretically the mantle is located where $\bar{u}_R = 0$, thus inducing the flow to switch polarity with respect to the cone apex between a downward and upward spiral. Since u_R is a function of the colatitude angle ϕ, we solve for the root of $\bar{u}_R = 0$ and call this inclination angle β. We find $\beta \cong 0.6\alpha$ with an absolute error that varies between 0.0066 and 0.11 deg for $1 \le \alpha \le 60^o$. The maximum error reaches 0.44 deg at $\alpha = 90^o$. The orientation of the mantle layer at 60% of the divergence angle is confirmed by Bradley and Pulling[36] in their investigation of hydraulic cyclones. The complete functional dependence of β and λ on α is illustrated in Fig. 5. Note that λ corresponds to the right-hand scale and varies between -4.24 and 1 for $1 \le \alpha \le 90^o$. As for the mantle location, both exact and approximate representations are overlaid and shown to be graphically indiscernible except near an improbable angle of 90%.

D. Equivalent Polar Values

In the interest of clarity, we convert our formulations into their polar cylindrical equivalents. The relation between spherical and cylindrical coordinates follows the standard transformation matrix,

$$\begin{cases} \bar{u}_r = \bar{u}_R\sin\phi + \bar{u}_\phi\cos\phi \\ \bar{u}_z = \bar{u}_R\cos\phi - \bar{u}_\phi\sin\phi \end{cases} \tag{60}$$

Substituting the values for the radial and latitudinal velocities, the cylindrical radial and axial velocities emerge as

$$\bar{u}_r = -\pi\sigma_o\Phi \quad \text{and} \quad \bar{u}_z = \pi\sigma_o\left(\lambda - \ln\Phi - 1\right) \tag{61}$$

The tangential velocity remains invariant in both coordinate systems. In order to fully convert the velocities, we substitute the relations $\bar{R} = \sqrt{\bar{r}^2 + \bar{z}^2}$, $\sin\phi = \bar{r}/\bar{R}$, $\cos\phi = \bar{z}/\bar{R}$, and $\phi = \tan^{-1}\left(\bar{r}/\bar{z}\right)$. We subsequently obtain the following assortment of dimensionless velocities,

$$\bar{u}_r = -\pi\sigma_o\left(\sqrt{1 + \zeta^2} - \zeta\right) \tag{62}$$

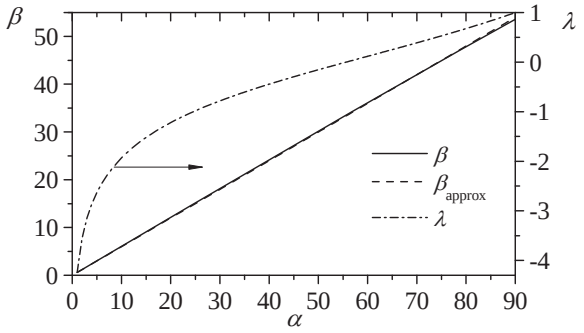

Figure 5. Mantle divergence angle β and characteristic parameter λ versus α.

$$\bar{u}_z = \pi\sigma_o\left[\lambda - \ln\left(\sqrt{1+\zeta^2} - \zeta\right) - 1\right] \tag{63}$$

$$\bar{u}_\theta = \frac{1}{\bar{r}}\sqrt{1+\left(\pi\sigma_o\bar{r}\right)^2\left[\lambda - \ln\left(\sqrt{1+\zeta^2} - \zeta\right) + \zeta\sqrt{1+\zeta^2} - \zeta^2 - 1\right]} \tag{64}$$

where $\zeta \equiv \bar{z}/\bar{r} = z/r$.

In the same vein, given that cylindrical coordinates can be simpler to visualize, we convert the spherical stream function, spherical radial velocity, and latitudinal velocity into polar form; we collect

$$\bar{\psi} = \tfrac{1}{2}\pi\sigma_o\bar{r}^2\left[\lambda - \ln\left(\sqrt{1+\zeta^2} - \zeta\right) + \zeta\sqrt{1+\zeta^2} - \zeta^2 - 1\right] \tag{65}$$

$$\bar{u}_R = \pi\sigma_o\left[\zeta\left(1+\zeta^2\right)^{-\frac{1}{2}}\left[\lambda - \ln\left(\sqrt{1+\zeta^2} - \zeta\right)\right] - 1\right] \tag{66}$$

$$\bar{u}_\phi = \pi\sigma_o\left\{\left(1+\zeta^2\right)^{-\frac{1}{2}}\left[\ln\left(\sqrt{1+\zeta^2} - \zeta\right) - \lambda\right] + \sqrt{1+\zeta^2} - \zeta\right\} \tag{67}$$

E. Radial Velocity Distribution

As mentioned in Section V.C, the spherical radial velocity, $\bar{u}_R$, controls the polarity of the flow. Simply, negative values imply downward motion whereas positive values correspond to an updraft (Fig. 1). In Fig. 4, the direction and location of the flow are delineated. The outer vortex is defined by the region in which $\bar{u}_R < 0$, thus transporting the fluid downwardly in a spiraling fashion; conversely, the positive $\bar{u}_R$ region within the inner vortex induces convection of the spinning fluid upwardly and out of the top.

Another feature that may be inferred from $\bar{u}_R$ concerns the physicality and behavior of the mantle. The conical mantle resides at the location where $\bar{u}_R = 0$. In Fig. 4, the line that demarcates the zero axis clearly shows the angle of the mantle for each α as deduced from Eq. (57). The mantle inclination angle remains constant throughout the cone, which in turn provides a constantly changing horizontal location as the axial position is vertically increased. This axial shifting is confirmed through Eq. (66) and may be observed in Fig. 6 where $\bar{u}_R$ is plotted at four axial locations of $z/L = 0.25,\ 0.50,\ 0.75,$ and 1, and for two divergence angles of $\alpha = 30°$ and $45°$. These curves help to delineate the inner and outer vortex regions in addition to the mantle expansion with either vertical movement or cone angle divergence.

It should be remarked that, in the absence of friction, the forced vortex region that characterizes cyclonic cores cannot be fully established without accounting for shear stresses. At the outset, the spherical radial velocity becomes unbounded as $\phi \to 0$. In a viscous flow, one predicts a core boundary layer to form at the centerline, thus mitigating the observed divergence in the velocity. One also expects a thin boundary layer to form at the sidewall, in fulfillment of the no slip requirement. Given that this article is focused on the complete presentation of exact Euler solutions, the approximate viscous analyses of the core and sidewall layers are deferred to a later study.

F. Latitudinal Velocity Distribution

By inspection of Eq. (58), the latitudinal velocity, $\bar{u}_\phi$, is seen to be solely dependent on the colatitude angle and the conical swirl number. Being somewhat akin to the radial velocity of the bidirectional vortex in a cylinder,[11] the latitudinal velocity for the spherical solution vanishes at both the core and the sidewall. These two velocities, $\bar{u}_\phi$

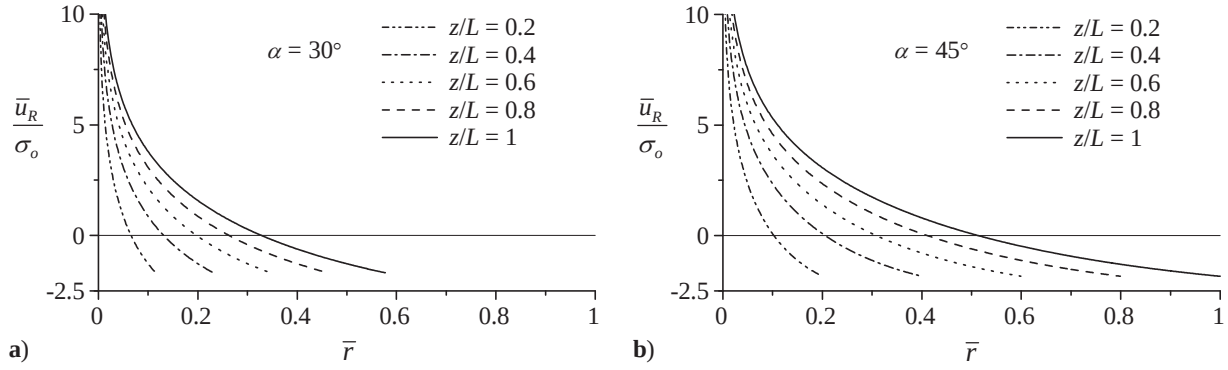

Figure 6. Radial velocity distribution shown at several axial positions and divergence angles of a) 30° and b) 45°.

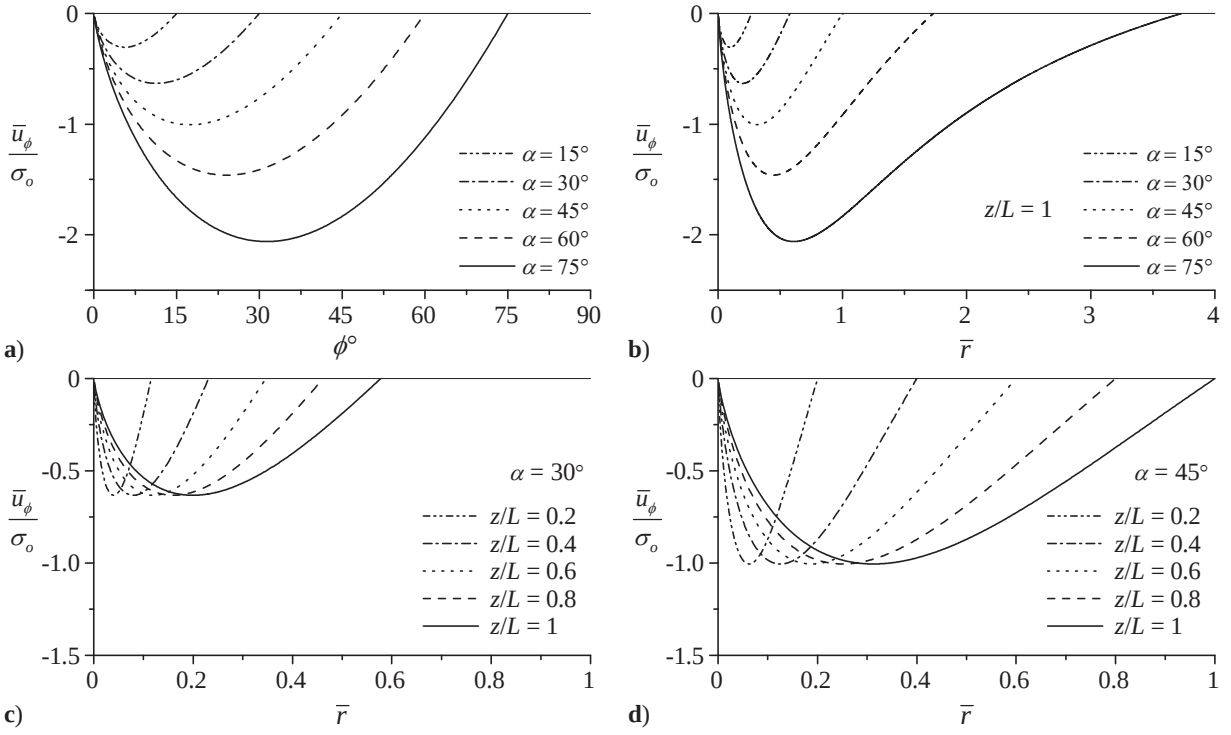

Figure 7. Latitudinal velocity over a) a range of α as a function of ϕ; b) a range of α at the top of the cone $(z = L)$; a range of axial positions and divergence angles of c) 30° and d) 45°.

and $\bar{u}_r$,[11] share the ability to link the inner and outer vortex regions through mass transport across the mantle. Since $\bar{u}_R = 0$ at $\phi = \beta$, the connection across the mantle depends only on the latitudinal velocity. The magnitude of $\bar{u}_\phi$ varies over a range of cone divergence angles, as shown in Fig. 7. However, these curves exhibit similar profiles. This is especially visible in Figs. 7c and 7d where the variation of $\bar{u}_\phi$ is shown at four axial cross-sections and two divergence angles. Everywhere between the axis and the wall, $\bar{u}_\phi$ retains a negative value that is indicative of inward flow toward the cone axis.

In the vicinity of the mantle, a maximum $|\bar{u}_\phi|$ can be determined. Interestingly, the maximum radial velocity of the bidirectional vortex in a cylinder also occurs within close proximity of the mantle. Here, the maximum $|\bar{u}_\phi|$ appears at a constant angle given that Eq. (58) is a function of ϕ only. This angle may be calculated from the derivative with respect to ϕ, namely,

$$\frac{\mathrm{d}u_\phi}{\mathrm{d}\phi} = 0 \quad \text{or} \quad \left[\left(\sin\phi\left\{\ln\left[\tan\left(\tfrac{1}{2}\phi\right)\right] - \lambda\right\} + \tan\left(\tfrac{1}{2}\phi\right)\right)\right]\Big|_{\phi_{\max}} = 0 \tag{68}$$

One gets

$$\cos\left(\phi_{\max}\right)\left\{\ln\left[\tan\left(\tfrac{1}{2}\phi_{\max}\right)\right] - \lambda\right\} + \tfrac{1}{2}\sec^2\left(\tfrac{1}{2}\phi_{\max}\right) + 1 = 0 \tag{69}$$

Hence for every α there exists a corresponding $\phi_{\max}$ which can be obtained numerically. A practically equivalent analytical root can be expressed in piecewise fashion,

$$\phi_{\max} = \begin{cases} 2\sqrt{\mathrm{pln}\left(-e^{2\lambda-3}\Xi\right)/\Xi}; & 0 < \alpha \le \alpha_0;\ \alpha_0 \simeq 0.38732\ (22.192\,\mathrm{deg}) \\ 2\sqrt{\mathrm{pln}\left(e^{2\lambda-3}\Xi\right)/\Xi}; & \alpha_0 < \alpha < \tfrac{1}{2}\pi \end{cases} \tag{70}$$

where $\Xi \equiv \frac{5}{3} + 4\lambda + 4\ln 2$. Alternatively, a simple asymptotic approximation for $\phi_{\max}$ may be extracted in degrees and written as:

$$\phi_{\max}[\mathrm{deg}] = 0.3376 + 0.3250\alpha + 0.001185\alpha^2\ [\mathrm{deg}]; \quad \alpha \ge 10\ \mathrm{deg} \tag{71}$$

As for the crossflow velocity, it coincides with the mantle location and may therefore be obtained through the simple substitution of $\phi = \beta$; one obtains

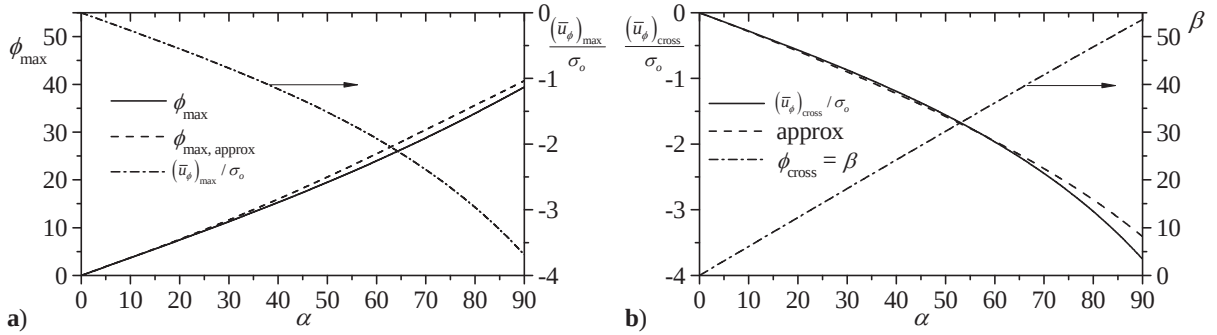

Figure 8. Variation with α of a) the maximum latitudinal speed and b) the crossflow velocity along with their corresponding loci.

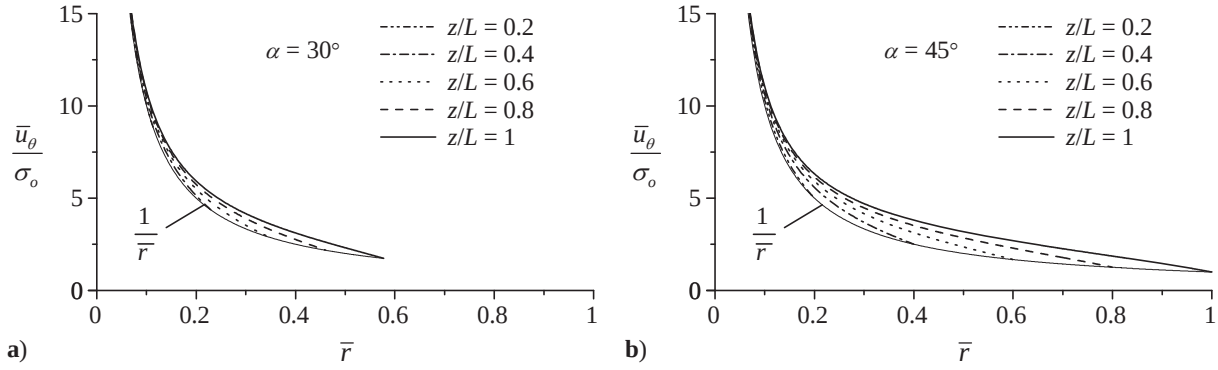

Figure 9. Tangential velocity distribution shown at several axial positions and divergence angles of a) 30° and b) 45°.

$$\left(\bar{u}_\phi\right)_{\text{cross}} = \pi\sigma_o\left(\sin\beta\left\{\ln\left[\tan\left(\tfrac{1}{2}\beta\right)\right]-\lambda\right\}+\tan\left(\tfrac{1}{2}\beta\right)\right) \cong -\left(0.511+0.06775\alpha+0.00917\alpha^4+0.00117\alpha^6\right)\pi\alpha\sigma_o \quad (72)$$

where α is in radian. The crossflow velocity along the mantle permits a constant supply of mass transport, or spillage as it were, from the outer, annular stream to the core region. Both $\left(\bar{u}_\phi\right)_{\max}/\sigma_o$ and $\phi_{\max}$, including the approximate expression given by Eq. (70), are illustrated in Fig. 8a. The crossflow velocity given in both exact and approximate forms by Eq. (72), are displayed side-by-side in Fig. 8b along with the mantle loci through which the crossing occurs. It may be seen that the maximum latitudinal velocity mirrors the crossflow velocity so closely that overlaying them can preclude visual discernment. This behavior is interesting because each of these velocities stands at a different angle, as shown in Fig. 8.

G. Tangential Velocity

Figure 9 illustrates the behavior of the swirl velocity in a polar plane shown at four equally spaced altitudes and two divergence angles of a) $\alpha = 30°$, and b) $\alpha = 45°$. As it may be inferred from the plots and confirmed through Eq. (64), $\bar{u}_\theta$ diminishes with the distance from the cone axis while bearing a weaker dependence on the inlet profile and spatial variation of the stream function. This grants the motion added sensitivity to the inlet conditions, especially when compared to the inviscid free vortex model of Vyas and Majdalani[10] (where $\bar{u}_\theta = \bar{r}^{-1}$ solely depends on the average inlet velocity). In both models, however, the purely inviscid form grows to unbounded levels at the core and fails to accommodate the velocity adherence condition that must be secured at the walls. This result is unsurprising, being a characteristic feature of most swirl dominated frictionless flows (see Bloor and Ingham,[29] Harvey,[37] or Leibovich[38-39]). The axial velocity shown in Fig. 10 exhibits similar features. Depending on the vertical distance from the apex, $\bar{u}_z$ crosses the oblique mantle while switching polarity.

H. Pressure and Vorticity Evaluation

The pressure may be directly evaluated from Euler's momentum equation. Using cylindrical coordinates for ease of referencing, we obtain:

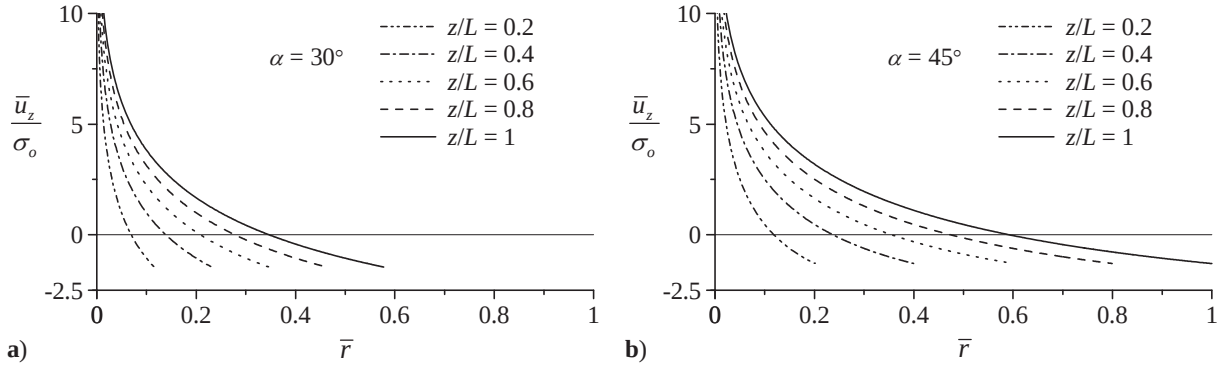

Figure 10. Axial velocity distribution shown at several axial positions and divergence angles of a) 30° and b) 45°.

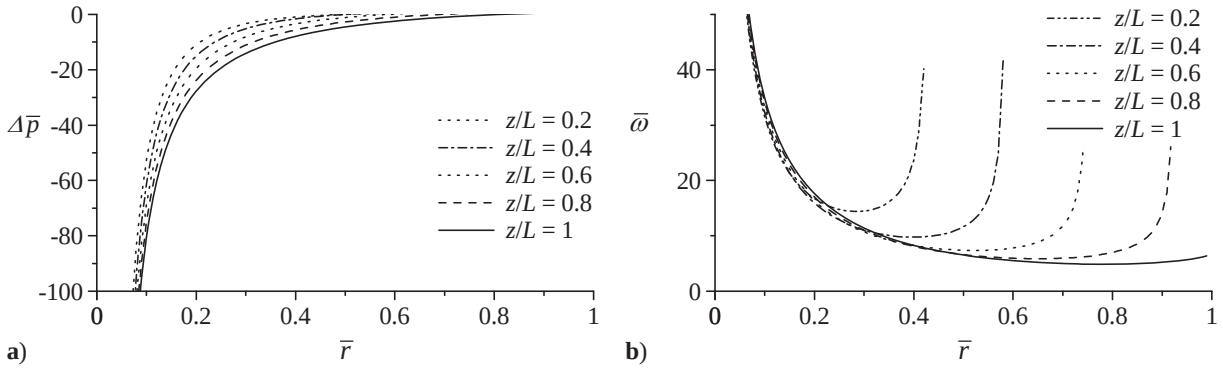

Figure 11. Radial distribution of a) pressure referenced to the apex and b) total vorticity at several axial positions and divergence angle of 45°.

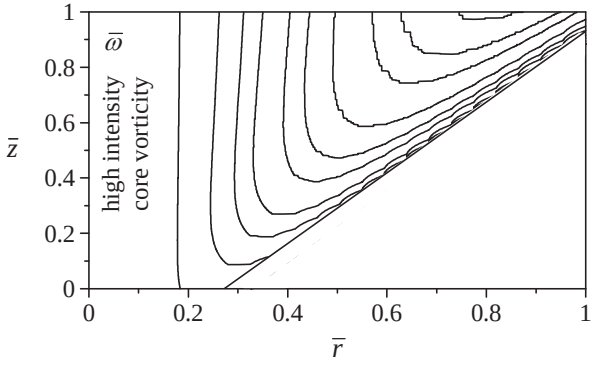

Figure 12. Isovorticity lines for a divergence angle of 45°.

$$\frac{\partial\overline{p}}{\partial\overline{r}} = \frac{1+\pi^2\overline{z}^2\sigma_o^2}{\overline{r}^3} + \pi^2\sigma_o^2\,\frac{\lambda-1+\operatorname{arcsinh}(\overline{z}/\overline{r})-\overline{z}^2/\overline{r}^2}{\overline{r}\sqrt{1+\overline{r}^2/\overline{z}^2}} = \frac{1}{\overline{r}^3} + \frac{\pi^2\sigma_o^2\zeta}{\overline{r}\sqrt{1+\zeta^2}}\left(\zeta\sqrt{1+\zeta^2}+\lambda-1+\operatorname{arcsinh}\zeta-\zeta^2\right) \quad (73)$$

$$\frac{\partial\overline{p}}{\partial\overline{z}} = \frac{\pi^2\sigma_o^2}{\sqrt{\overline{r}^2+\overline{z}^2}}\left\{\frac{\overline{z}^2}{\overline{r}^2}-\frac{\overline{z}}{\overline{r}}\sqrt{1+\frac{\overline{z}^2}{\overline{r}^2}}-\lambda-\operatorname{arcsinh}(\overline{z}/\overline{r})+1\right\} = \frac{\pi^2\sigma_o^2}{\overline{r}\sqrt{1+\zeta^2}}\left(\zeta^2-\zeta\sqrt{1+\zeta^2}-\lambda-\operatorname{arcsinh}\zeta+1\right) \quad (74)$$

Taking the normalized $\overline{p}_0$ as our baseline at the apex of the cone, Eqs. (73)-(74) may be partially integrated to yield, $\Delta\overline{p} = \overline{p} - \overline{p}_0$, where

$$\Delta\bar{p} = \frac{-1+\pi^2\bar{z}(\sqrt{\bar{r}^2+\bar{z}^2}-\bar{z})\sigma_o^2 - \pi^2\bar{r}^2\sigma_o^2\,\mathrm{arcsinh}(\bar{z}/\bar{r})\left[2\lambda+\mathrm{arcsinh}(\bar{z}/\bar{r})-1\right]}{2\bar{r}^2}$$

$$= -\frac{1}{2\bar{r}^2} + \frac{1}{2}\pi^2\sigma_o^2\left\{\zeta\sqrt{1+\zeta^2} - \zeta^2 - \mathrm{arcsinh}\zeta\left(2\lambda - 1 + \mathrm{arcsinh}\zeta\right)\right\} \tag{75}$$

Figure 11a illustrates the behavior of $\Delta\bar{p}$ at several axial stations and $\sigma_o = 1$. It is clear that the pressure variation is dominated by its $-\frac{1}{2}\bar{r}^{-2}$ leading order term, a result that is also characteristic of the bidirectional vortex in a cylinder.[10] Note that the pressure difference is negligible at the wall and largest near the centerline.

Vorticity in this problem may also be evaluated using $\bar{\boldsymbol{\omega}} = \nabla\times\bar{\boldsymbol{u}}$. We obtain

$$\bar{\omega}_r = -\frac{\pi^2\sigma_o^2}{(\zeta+\sqrt{1+\zeta^2})\sqrt{1+\pi^2\bar{r}^2\sigma_o^2\left[\lambda-1+\mathrm{arcsinh}\zeta+\zeta/\left(\zeta+\sqrt{1+\zeta^2}\right)\right]}} \tag{76}$$

$$\bar{\omega}_\theta = \frac{\pi\sigma_o}{\bar{r}}; \qquad \bar{\omega}_z = \frac{\pi^2\sigma_o^2\left(\lambda-1+\mathrm{arcsinh}\zeta\right)}{\sqrt{1+\pi^2\bar{r}^2\sigma_o^2\left[\lambda-1+\mathrm{arcsinh}\zeta+\zeta/\left(\zeta+\sqrt{1+\zeta^2}\right)\right]}} \tag{77}$$

The radial variation of the total vorticity is displayed in Fig. 11b at several fixed locations. The vorticity lines confirm the duality of radial positions that yield the same value of $\bar{\omega}$ at given $\bar{z}$. This may be attributed to the transport of vorticity along looping streamlines. As for the magnitude of vorticity, it increases as the axis of rotation is approached, especially inside an approximately 20% radius. Here too, the over-amplification at the origin is caused by the absence of viscous damping.

To compensate for the deficiencies associated with our Euler solution, the addition of appropriate viscous corrections have to be judiciously considered through the use of boundary layer treatment that tightly intertwines with asymptotic analysis. With the stream function and velocities at hand, it is hoped that viscous effects will be addressed in forthcoming study, in addition to other possible forms of solution. Numerical and experimental investigations are also hoped to be achieved for the purpose of verification and validation.

VI. Conclusions

This work revisits the problem arising in the context of a bidirectional vortex in a conical chamber. Immediate applications include industrial cyclone separators or modified versions of the vortex liquid and hybrid rocket engines. Starting with the spherical Bragg-Hawthorne equation, an exact and verifiable Euler solution is derived that overcomes some of the deficiencies and limitations of previous mathematical models of conical cyclones. Our results are not only presented in spherical coordinates, but also in polar cylindrical form to facilitate cross-referencing. Through a judicious choice of normalization parameters a universal, self-similar formulation is produced that is independent of the cone's vertical dimension. The ensuing analysis enables us to identify key characteristic parameters such as: (1.) the mantle inclination at 60% of the cone's divergence half-angle; (2.) the crossflow velocity along the mantle interface $\left(\bar{u}_\phi\right)_{\text{cross}}$; and (3.) the maximum latitudinal velocity $\left|\bar{u}_\phi\right|$ and its locus $\phi_{\max}$. The latter is reminiscent of the radial velocity in a right-cylindrical chamber. It is interesting that our theoretical prediction for β is fully supported by experimental measurements.[36] On this note, several asymptotic approximations are provided and some appear in a piecewise form that depends on a cutoff half-angle of 22.2 deg.

After expressing the stream function in polar cylindrical form, $\bar{\psi} = \frac{1}{2}\pi\sigma_o\bar{r}(\lambda - \ln\Phi - \Phi\sqrt{1+\zeta^2})$, we are able to deduce the fundamental expression linking the tangential angular momentum, $\bar{\mathrm{B}} = \bar{r}\,\bar{u}_\theta = \sqrt{1+2\pi\sigma_o\bar{\psi}}$, and the stream function. This function plays a central role in the Bragg-Hawthorne equation as it leads to a solution that is capable of satisfying the problem's physical constraints. It thus complements previous studies such as those by Bloor and Ingham[29] and Majdalani and Rienstra.[11] In hindsight, this form could have been posited at the beginning of the analysis to precipitate the solution more rapidly. Similar forms of $\bar{\mathrm{B}}$ may be substituted in seeking solutions to this general class of problems including $\mathrm{B} = B_0, \sqrt{B_0+B_1\psi}, \sqrt{B_0+B_1\psi^{\pm m}}, B_0\psi, B_0\psi^{\pm m}, \ldots$ Along similar lines, a generalization beyond $\mathrm{H} = \text{const}$ may be attempted in the search for more elaborate flow motions. Models exhibiting variable $\mathrm{H} = H_0, \sqrt{H_0+H_1\psi}, \sqrt{H_0+H_1\psi^{\pm m}}, H_0\psi, H_0\psi^{\pm m}, \ldots$ and combinations thereof may be worthwhile to consider. While Majdalani and Rienstra[11] have initiated the quest for alternate flowfield representations, including nonlinear relations between vorticity and $\bar{\psi}^m$, much exploratory work remains ahead. The resulting approximations may find suitable applications beyond the realm of injection and swirl driven motions.

Acknowledgments

This project was funded by the National Science Foundation through grant No. CMMI-0353518, Dr Eduardo A. Misawa, Program Director.

References

[1]Majdalani, J., and Vyas, A. B., "Rotational Axisymmetric Mean Flow for the Vortex Injection Hybrid Rocket Engine," AIAA Paper 2004-3475, July 2004.

[2]Knuth, W. H., Chiaverini, M. J., Sauer, J. A., and Gramer, D. J., "Solid-Fuel Regression Rate Behavior of Vortex Hybrid Rocket Engines," *Journal of Propulsion and Power*, Vol. 18, No. 3, 2002, pp. 600-609.

[3]Knuth, W. H., Chiaverini, M. J., Gramer, D. J., and Sauer, J. A., "Final Report on Gas-Fed, Vortex Injection Hybrid Rocket Engine- a Phase II SBIR Project," Orbital Technological Corporation, NASA Contract No. NAS8-97015 Rept. OTC-GS055-FR-99-1, Madison, Wisconsin, January 1999.

[4]Knuth, W. H., Chiaverini, M. J., Gramer, D. J., and Sauer, J. A., "Final Report on Vortex Combustion Ramjet- a Phase I SBIR Project," Orbital Technological Corporation, NASA Contract No. NAS3-99039 Rept. OTC-GS075-FR-99-1, June 1999.

[5]Knuth, W. H., Chiaverini, M. J., Gramer, D. J., and Sauer, J. A., "Solid-Fuel Regression Rate and Combustion Behavior of Vortex Hybrid Rocket Engines," AIAA Paper 99-2318, July 1999.

[6]Knuth, W. H., Chiaverini, M. J., Gramer, D. J., Sauer, J. A., St. Clair, C. P., Whitesides, R. H., and Dill, R. A., "Preliminary Computational Fluid Dynamics Analysis of the Vortex Hybrid Rocket Chamber and Nozzle Flowfield," AIAA Paper 98-3351, July 1998.

[7]Knuth, W. H., Gramer, D. J., Chiaverini, M. J., and Sauer, J. A., "Development and Testing of Vortex Driven, High Regression Rate Hybrid Rocket Engines," AIAA Paper 98-3507, July 1998.

[8]Knuth, W. H., Chiaverini, M. J., Gramer, D. J., and Sauer, J. A., "Experimental Investigation of a Vortex-Driven High-Regression Rate Hybrid Rocket Engine," AIAA Paper 98-3348, July 1998.

[9]Knuth, W. H., Bemowski, P. A., Gramer, D. J., Majdalani, J., and Rothbauer, W. J., "Gas-Fed, Vortex Injection Hybrid Rocket Engine," NASA Marshall Space Flight Center, SBIR Phase I Final Technical Rept. NASA/MSFC Contract NAS8-40679, Huntsville, AL, August 1996.

[10]Vyas, A. B., and Majdalani, J., "Exact Solution of the Bidirectional Vortex," *AIAA Journal*, Vol. 44, No. 10, 2006, pp. 2208-2216.

[11]Majdalani, J., and Rienstra, S. W., "On the Bidirectional Vortex and Other Similarity Solutions in Spherical Coordinates," *Journal of Applied Mathematics and Physics (ZAMP)*, Vol. 58, No. 2, 2007, pp. 289-308.

[12]Vyas, A. B., Majdalani, J., and Chiaverini, M. J., "The Bidirectional Vortex. Part 1: An Exact Inviscid Solution," AIAA Paper 2003-5052, July 2003.

[13]Vyas, A. B., Majdalani, J., and Chiaverini, M. J., "The Bidirectional Vortex. Part 2: Viscous Core Corrections," AIAA Paper 2003-5053, July 2003.

[14]Vyas, A. B., Majdalani, J., and Chiaverini, M. J., "The Bidirectional Vortex. Part 3: Multiple Solutions," AIAA Paper 2003-5054, July 2003.

[15]Majdalani, J., "Vortex Injection Hybrid Rockets," *Fundamentals of Hybrid Rocket Combustion and Propulsion*, edited by K. Kuo and M. J. Chiaverini, AIAA Progress in Astronautics and Aeronautics, Washington, DC, 2007, pp. 247-276.

[16]Anderson, M. H., Valenzuela, R., Rom, C. J., Bonazza, R., and Chiaverini, M. J., "Vortex Chamber Flow Field Characterization for Gelled Propellant Combustor Applications," AIAA Paper 2003-4474, July 2003.

[17]Rom, C. J., Anderson, M. H., and Chiaverini, M. J., "Cold Flow Analysis of a Vortex Chamber Engine for Gelled Propellant Combustor Applications," AIAA Paper 2004-3359, July 2004.

[18]Fang, D., Majdalani, J., and Chiaverini, M. J., "Simulation of the Cold-Wall Swirl Driven Combustion Chamber," AIAA Paper 2003-5055, July 2003.

[19]Fang, D., Majdalani, J., and Chiaverini, M. J., "Hot Flow Model of the Vortex Cold Wall Liquid Rocket," AIAA Paper 2004-3676, July 2004.

[20]ter Linden, A. J., "Investigations into Cyclone Dust Collectors," *Proceedings of the Institution of Mechanical Engineers*, Vol. 160, 1949, pp. 233-251.

[21]Kelsall, D. F., "A Study of Motion of Solid Particles in a Hydraulic Cyclone," *Transactions of the Institution of Chemical Engineers*, Vol. 30, 1952, pp. 87-103.

[22]Smith, J. L., "An Experimental Study of the Vortex in the Cyclone Separator," *Journal of Basic Engineering-Transactions of the ASME*, 1962, pp. 602-608.

[23]Smith, J. L., "An Analysis of the Vortex Flow in the Cyclone Separator," *Journal of Basic Engineering-Transactions of the ASME*, 1962, pp. 609-618.
[24]Peng, W., Hoffmann, A. C., and Dries, H., "Separation Characteristics of Swirl-Tube Dust Separators," *AIChE Journal*, Vol. 50, No. 1, 2004, pp. 87-96.
[25]Hu, L. Y., Zhou, L. X., Zhang, J., and Shi, M. X., "Studies of Strongly Swirling Flows in the Full Space of a Volute Cyclone Separator," *AIChE Journal*, Vol. 51, No. 3, 2005, pp. 740-749.
[26]Cortes, C., and Gil, A., "Modeling the Gas and Particle Flow inside Cyclone Separators," *Progress in Energy and Combustion Science*, Vol. in Press, 2007.
[27]Fontein, F. J., and Dijksman, C., *Recent Developments in Mineral Dressing*, Institution of Mining and Metallurgy, London, 1953, p. 229.
[28]Bloor, M. I. G., and Ingham, D. B., "Theoretical Investigation of the Flow in a Conical Hydrocyclone," *Transactions of the Institution of Chemical Engineers*, Vol. 51, No. 1, 1973, pp. 36-41.
[29]Bloor, M. I. G., and Ingham, D. B., "The Flow in Industrial Cyclones," *Journal of Fluid Mechanics*, Vol. 178, No. 1, 1987, pp. 507-519.
[30]Hsieh, K. T., and Rajamani, R. K., "Mathematical Model of the Hydrocyclone Based on Physics of Fluid Flow," *AIChE Journal*, Vol. 37, No. 5, 1991, pp. 735-746.
[31]Hoekstra, A. J., Derksen, J. J., and Van den Akker, H. E. A., "An Experimental and Numerical Study of Turbulent Swirling Flow in Gas Cyclones," *Chemical Engineering Science*, Vol. 54, No. 13, 1999, pp. 2055-2065.
[32]Derksen, J. J., and Van den Akker, H. E. A., "Simulation of Vortex Core Precession in a Reverse-Flow Cyclone," *AIChE Journal*, Vol. 46, No. 7, 2000, pp. 1317-1331.
[33]Zhao, J. Q., and Abrahamson, J., "The Flow in Conical Cyclones," in *Second International Conference on CFD in the Minerals and Process Industries* CSIRO, Melbourne, Australia, 1999, pp. 497-502.
[34]Majdalani, J., "Exact Eulerian Solutions of the Cylindrical Bidirectional Vortex," AIAA Paper 2009-5307, August 2009.
[35]Bragg, S. L., and Hawthorne, W. R., "Some Exact Solutions of the Flow through Annular Cascade Actuator Disks," *Journal of the Aeronautical Sciences*, Vol. 17, No. 4, 1950, pp. 243-249.
[36]Bradley, D., and Pulling, D. J., "Flow Patterns in the Hydraulic Cyclone and Their Interpretation in Terms of Performance," *Transactions of the Institution of Chemical Engineers*, Vol. 37, 1959, pp. 34-45.
[37]Harvey, J. K., "Some Observations of the Vortex Breakdown Phenomenon," *Journal of Fluid Mechanics*, Vol. 14, No. 4, 1962, pp. 585-592.
[38]Leibovich, S., "The Structure of Vortex Breakdown," *Annual Review of Fluid Mechanics*, Vol. 10, 1978, pp. 221-246.
[39]Leibovich, S., "Vortex Stability and Breakdown: Survey and Extension," *AIAA Journal*, Vol. 22, No. 9, 1984, pp. 1192-1206.